On the improved point-to-point calculations for noise mapping in shielded urban areas

Maarten Hornikx[a]
Jens Forssén[b]
Department of Civil and Environmental Engineering, Chalmers University of Technology
Division of Applied Acoustics, SE-41296 Gothenburg, Sweden

Mikael Ögren[c]
Department of Environmental and Traffic Analysis, VTI, Gothenburg, Sweden

Dick Botteldooren[d]
Timothy van Renterghem[e]
Weigang Wei[f]
Department of Information Technology, Ghent University, Ghent, Belgium

Erik Salomons[g]
Institute of Applied Physics, TNO, Delft, Netherlands

Noise mapping of urban areas according to standardized engineering calculation methods systematically results in an underestimation of noise levels at areas shielded from direct exposure to noise, such as inner yards. In these methods, road traffic lanes are represented by point sources and noise levels are computed utilizing point-to-point propagation paths. For a better prediction of noise levels in shielded urban areas, the attenuation terms describing these propagation paths are extended by terms including geometrical aspects of the urban environment both in the source and in the receiver area. In the present work, it

---

[a]email: maarten.hornikx@chalmers.se
 Also affiliated with: Building Physics and Services, Eindhoven University of Technology, Eindhoven, Netherlands
[b]email: jens.forssen@chalmers.se
[c]email: mikael.ogren@vti.se
[d]email: dick.botteldooren@intec.ugent.be
[e]email: timothy.van.renterghem@intec.ugent.be
[f]email: weigang@intec.ugent.be
[g]email: erik.salomons@tno.nl

has been studied to what extent these terms may be treated as being independent of the source-receiver distance. Also, the validity of treating the propagation path in a 2D plane rather than in 3D is investigated. Results obtained from a wave-based acoustic propagation model have been used for this assessment.

1   INTRODUCTION

According to the European Noise Directive (END) 2002/49/EC, European cities have to produce noise maps and exposure distributions based on noise levels at the façades of dwellings.[1] In addition, the END indicates that cities should quantify how many persons have access to a quiet façade, and that quiet urban areas should be protected. Current engineering methods for computing these noise maps work well for the areas directly exposed to noise, but have been shown to underestimate the levels at areas shielded from direct exposure as quiet façades and quiet urban areas.[2,3] Therefore, an acoustic calculation model that is suitable for quiet façades and quiet urban areas is being proposed.[4] This method should at the same time be suitable for engineering use. The proposed method extends the engineering formulae for screening by noise barriers and can be written as:

$$L_p(\vec{x}_r) = \sum_{i=1}^{N} \left(L_w + A_{free} + A_{bar} + A_{can} + A_{inter} + A_{meteo} \right)_i,$$

with

$$A_{can} = A_s + A_r \quad for \quad \left| \vec{x}_{s,\perp} - \vec{x}_{r,\perp} \right| > x_{unc}$$

(1)

with

Source and receiver coordinates $\vec{x}_s = \left(x_s, y_s, z_s \right)$ and $\vec{x}_r = \left(x_r, y_r, z_r \right)$ [m]

Source and receiver coordinates in the horizontal plane $\vec{x}_{s,\perp} = \left(x_s, y_s \right)$ and $\vec{x}_{r,\perp} = \left(x_r, y_r \right)$ [m]

x_{unc} = distance of uncoupling [m]
L_p = sound pressure level in 1/3 octave bands, [dB]
N = number of contributing sources [-]
L_w = source power level [dB]
A_{free} = 3D free field divergence [dB]
A_{bar} = barrier attenuation [dB].

The additional proposed terms are:
A_{can} = attenuation caused by multiple reflections in the source and receiver environments [dB]
A_s = attenuation caused by multiple reflections in the source environment [dB]
A_r = attenuation caused by multiple reflections in the receiver environment [dB]
A_{inter} = attenuation caused by the diffraction into intermediate canyons [dB]
A_{meteo}= attenuation due to meteorological effects [dB].

For $\left| \vec{x}_{s,\perp} - \vec{x}_{r,\perp} \right| > x_{unc}$, the horizontal source-receiver distance is large enough such that A_{can} can be split in the uncoupled terms A_s and A_r. This is favorable since A_s and A_r can then be assigned to source and receiver positions independently, and can be used for multiple source-receiver paths. For $\left| \vec{x}_{s,\perp} - \vec{x}_{r,\perp} \right| < x_{unc}$, A_{can} is not split into A_s and A_r and should be computed as a single term. In the absence of reflections in the source and receiver environment, A_{can} reduces to 0. For deriving simple expressions of A_{can} for a range of urban configurations, detailed two-dimensional (2D)

point-to-point calculations using a wave-based sound propagation method have previously been proposed.[4] To assess the validity of these calculations, as well as the proposed splitting of A_{can} into A_s and A_r, this paper contains two key parts:

1) Assessing the minimum distance x_{unc} for the terms A_s and A_r to be regarded as uncoupled. Further, it will be investigated whether A_s and A_r are independent on $\left| \vec{x}_{s,\perp} - \vec{x}_{r,\perp} \right|$.

2) Investigation of the accuracy of computing A_s and A_r by a 2D approach.

All computations in this paper are performed using the pseudo-spectral time-domain method (PSTD), a wave-based method that is efficient enough to handle the studied urban geometries.[5]

2   CONFIGURATIONS OF STUDY AND MODELING APPROACH

Figure 1 shows the 2D configurations studied in this paper. Urban configurations are considered, with source and receivers located in street canyons. Configuration *can* represents the canyon-to-canyon configuration with a single noise source in one street canyon and receiver positions in another canyon. All façades are considered to be equal and have six depressions, corresponding to the window surfaces. The other façade parts represent brickwork. Window and brickwork materials are modeled by a real normalized impedance of $Z_n=77$ and $Z_n=10$ respectively. All other surfaces are acoustically rigid. The current work is restricted to fixed canyon dimensions with values $H=W=19.2$ m (see Figure 1). The term A_{can} in Eqn. (1) for configuration *can* is computed by the sound pressure level relative to the level for configuration *can,ref*, i.e. the single thick barrier case (see Figure 1). As such, A_{can} only includes contributions from source to receiver including at least one façade reflection. Further, in order to investigate whether source and receiver environment effects may be treated as being uncoupled, configurations *s* and *r* as shown in Figure 1 are modeled to compute A_s and A_r. In current engineering methods including the first three terms on the right side of Eqn. (1), A_{bar} is computed by an approximate diffraction method, see e.g.[6] To comply with these engineering methods, the reference configurations for the term A_{can} are computed by similar method. In particular, the 3D Hadden and Pierce (HP) model to compute diffraction around a wedge has been used.[7] For the 2D solution of the reference configurations, the equivalence of the sound pressure level relative to free field propagation between a coherent line source and a point source, as proposed in Ref. 8, is used here. We note that by using this diffraction model, the façades are treated as flat and rigid in the reference configurations. We consider a frequency range up to 1.6 kHz in this work.

To compute sound pressure levels for the configurations of Figure 1, the PSTD method has been used to solve the wave equation.[5] Within this method, reflection free boundaries have been modeled by including a perfectly matched layer (PML). For some of the calculations, a hybrid computational approach is adopted. This approach divides the computational domain in a part where a numerical solution is needed and a part where an analytical solution of the wave equation is available. The PSTD method is used to solve the wave equation in the former part. The pressure and normal velocity components are computed by the PSTD method over a vertical line at $x=W/2+2$ m, see Figure 2(b). Then, the solution in the latter part is computed by applying the Kirchhoff-Helmholtz (KH) integral method to the vertical line at $x=W/2+2$ m in Fig. 2(b). This integral method relies on Green's functions which are known at the right side of the vertical line at $x=W/2+2$ m, and a homogeneous and non-moving medium is assumed. With this hybrid approach, a higher numerical efficiency is obtained compared to applying the PSTD method to the complete domain. To keep accuracy at the far receiver positions as considered here, the height of the integration plane z_{KH} at $x=W/2+2$ m should be sufficient. The accuracy of the KH-approach is therefore investigated for an analytical case of a source over a rigid ground surface, see Figure 3(a), for $x=200$ m and with $z_{KH}=29.6$ m. The computed solution at x_{KH} is tapered near

the top by a super-Gaussian window to avoid diffraction from the edge when integrating over the plane, i.e. for the pressure:

$$p(x_{KH}, z) = \begin{cases} G(x_{KH}, z \mid 0,0)e^{-\alpha(z-z_0)^6} & for \;\; z_0 < z < z_{KH} \\ G(x_{KH}, z \mid 0,0) & for \;\; 0 < z < z_0 \end{cases},$$

(2)

with $G(x_{KH},z|0,0)$ the 2D Green's function from the source to the KH-plane. Figure 3(b) shows the error as a function of the 1/3 octave band, which is negligible above 50 Hz. The value of z_{KH}=29.6 m is therefore used for further calculations in this paper.

3   ADDITIVITY OF A_s AND A_r AND DISTANCE DEPENDENCE

In this part of the study, we rely on 2D PSTD calculations. In Section 4, 3D results are evaluated and the limitation of the 2D results will be discussed there. Whereas all variables of Eqn. (1) intrinsically reflect 3D results, all variables here are indexed by a subscript 2D to highlight that presented results correspond to 2D results. Two major issues need to be treated here:

1)   In the engineering approach of Eqn. (1), it would be of interest to have $A_{s,2D}$ and $A_{r,2D}$ as distance independent (but frequency dependent) numbers. The question is therefore for what source-receiver distances these numbers can be approximated as constants.

2)   The distance x_{unc} for which correction terms $A_{s,2D}$ and $A_{r,2D}$ are uncoupled, with $A_{s,2D}=L_{p,s,2D}$ $-L_{p,s,ref,2D}$, $A_{r,2D}=L_{p,r,2D}$ $-L_{p,r,ref,2D}$, and $L_{p,q,2D}$ the sound pressure level computed for the 2D configuration q of Figure 1, where q stands for s, s,ref, r or r,ref.

3.1 Distance dependence

For configurations s and s,ref of Figure 1, $A_{s,2D}$ is computed using the hybrid computational technique as described above. Figure 4(a) shows $\Delta A_{s,2D}(x)=A_{s,2D}(x)-A_{s,2D}(10W)$ as a function of the receiver distance $x=(Q+W)/2$ and 1/3 octave bands. It illustrates that the source environment effect approaches a constant value for larger distances and is rather independent of frequency, at least above 100 Hz. It would be convenient when $A_{s,2D}$ could be considered as distance independent for $x>x_{unc}/2$, i.e. $Q+W>x_{unc}$. We therefore approximate both configurations s and s,ref as equivalent free field situations, such that:

$$A_{s,2D}(x,f) = L_{p,s,2D}(x,f) - L_{p,s,ref,2D}(x,f) \approx 10\log_{10}\left(\frac{B_{s,2D}}{x-x_{ES}}\right) - 10\log_{10}\left(\frac{B_{s,ref,2D}}{x-x_{ES,ref}}\right)$$
$$= A'_{s,2D} + 10\log_{10}\left(\frac{x-x_{ES,ref}}{x-x_{ES}}\right).$$

(3)

Here, $B_{s,2D}$ and $B_{s,ref,2D}$ are the amplitudes of the equivalent sources and x_{ES} and $x_{ES,ref}$ (both smaller than x) are the equivalent source positions (ES) found by fitting. Figures 4(c) and 4(d) show $\Delta B_{q,2D}(x)=B_{q,2D}(x)-B_{q,2D}(10W)$, with $B_{q,2D}=L_{p,q,2D}+10\log_{10}(x-x_q)$, with q the configuration s or s,ref and $x_{ES}=W/4$ m and $x_{ES,ref}=W/2$ m. The latter can be understood as that cylindrical spreading originates from the diffraction edge. Due to larger travel distance of contributions from façade reflections, $x_{ES}<x_{ES,ref}$. Obviously, the equivalent free field representation works well to

obtain coefficients B which are rather independent on x. With the given values of x_{ES} and $x_{ES,ref}$, $\Delta A'_{s,2D}$ is computed from Eqn. (3) using $A'_{s,2D}(x)=A_{s,2D}(x)-10\log_{10}|(x-x_{ES,ref})/(x-x_{ES})|$ and is plotted in Figure 4(b). We may conclude that from $x\geq 2W$, i.e. $Q\geq 3W$, treating $A'_{s,2D}$ as a distance independent number is a good assumption, leading to an error smaller than 0.5 dB at the 1/3 octave bands above 63 Hz.

For the configurations r and r,ref, a similar equivalent free field approach as for source configurations has been followed, i.e. with an equivalent receiver (ER), and the latter term of Eqn. (3) then reads $10\log_{10}|x_{ER,ref}/x_{ER}|$. The results for $\Delta B_{q,2D}(2W)$, with $q=r$ or $q=r,ref$ and with x the position of the central axis of the canyon, are illustrated in Figures 5(a) and (b) as a function of the receiver position and the 1/3 octave band. The chosen values for $x_{ER}=x-W/4$ and $x_{ER,ref}=x-W/2$ are taken equal for all receiver positions and do perform well for most receiver positions. The results of $\Delta A'_{r,2D}(2W)$ are plotted in Figure 5(c), showing only deviations above 0.5 dB for the highest frequencies or highest receiver positions in the façade furthest away from the source.

3.2 Additivity of A_s and A_r

Since both source and receiver environments do not have an analytical solution in configurations can and can,ref of Figure 1, these cases have been computed by single PSTD computations. As for the separate configurations of Section 3.1, configurations can and can,ref may be represented by equivalent free field analogies, with equivalent sources and receivers. Their location is taken according to Section 3.1, i.e. $x_{ES}=W/4$, $x_{ES,ref}=W/2$, $x_{ER}=x-W/4$ and $x_{ER,ref}=x-W/2$, and for $A'_{can,2D}$, the last term of Eqn. (3) becomes $10\log_{10}|(x_{ER,ref}-x_{ES,ref})/(x_{ER}-x_{ES})|$. To verify the relation $A'_{can,2D}=A'_{s,2D}+A'_{r,2D}$, the broadband difference $(A'_{s,2D}+A'_{r,2D})-A'_{can,2D}$ is plotted in Figure 6(a) as a function of x. For the source spectrum, the A-weighted sound power spectrum L_w=63, 75, 87, 95, 97, 104 dB for the octave bands 32-1000 Hz has been used, representing urban road traffic noise. The plotted results have arithmetically been averaged over all receiver positions. We notice a close agreement for all investigated values of x. In Figure 6(b), the frequency dependent values of arithmetically averaged receiver position values of $A'_{s,2D}+A'_{r,2D}$ and $A'_{can,2D}$ are plotted for $x=10W$. It shows the high amplification of the levels due to the multiple reflections compared to the single diffraction and highlights that $(A'_{s,2D}+A'_{r,2D})-A'_{can,2D}$ values are rather insignificant. We note that for $x>2W$, $|(A'_{s,2D}+A'_{r,2D})-A'_{can,2D}|<0.5$ dB. This number seems to be a good choice for x_{unc} when considering results averaged over the receiver positions. However, figures 4 and 5 indeed indicate that distance independence of terms $A'_{s,2D}$ and $A'_{r,2D}$ may be assumed for $Q>3W$, corresponding to $x=2x_{unc}$ for the total source-to-receiver distance.

4   2D VERSUS 3D APPROACH

The terms A_s and A_r of the extended engineering model of Eqn. (1) are favorably obtained when calculations underlying them are allowed to rely on 2D simplifications. The accuracy of this approach is studied here and we focus on $Q>W$, i.e. for which $A_{can,2D}\approx A_{s,2D}+A_{r,2D}$. Further, as was shown in Section 3 that $A_{s,2D}$ and $A_{r,2D}$ can be written as distance dependent terms and distance independent numbers $A'_{s,2D}$ and $A'_{r,2D}$, we will here search for the relation between $A'_{s,2D}$ and $A'_{r,2D}$ at one hand, and A'_s and A'_r at the other hand.

As for the 2D configurations, the terms A_s and A_r are also proposed to be written as a sum of distance independent and distance dependent terms, e.g. for A_r

$$A_r(\vec{x}_\perp, f) = L_{p,r}(\vec{x}_\perp, f) - L_{p,r,ref}(\vec{x}_\perp, f) \approx 10\log_{10}\left(\frac{B_r}{\left|\vec{x}_{ER,\perp}\right|^2}\right) - 10\log_{10}\left(\frac{B_{r,ref}}{\left|\vec{x}_{ER,ref,\perp}\right|^2}\right),$$

$$= A'_{r,} + 20\log_{10}\left(\frac{\left|\vec{x}_{ER,ref,\perp}\right|}{\left|\vec{x}_{ER,\perp}\right|}\right),$$

(4)

with $\vec{x}_{ER,\perp} = (x+W, y)$, $\vec{x}_{ER,ref,\perp} = (x, y)$. For configurations r and with $y_s = y = 0$ m, the numbers $\Delta B_r(x=2W)$ and $\Delta B_{r,ref}(x=2W)$ are plotted in Figures 5(d) and 5(e). Whereas the $\Delta B_{r,ref}(2W)$ results indicate a distance independence beyond $x=2W$ for most positions, $\Delta B_r(2W)$ shows that distance independence occurs from a larger distance for configuration r. $\Delta A'_r$ is therefore plotted for $x=4W$ in Figure 5(f), showing that the distance of $4W$ is approximately needed for a distance independence of A'_r. The broadband $A'_{r,2D}(x)-A'_r(x)$ values are plotted in Figure 7(a), arithmetically averaged over the receiver positions, illustrating a close agreement, even down to $x=2W$. The results at $x=10W$ as a function of frequency in Figure 7(b) show as well a good agreement.

The effects of the y-position of the receiver outside an infinitely long canyon with the source at $y_s=0$ are computed in 3D and are compared to results from a *projected* 2D approach, as illustrated in Figure 8. The *projected* 2D approach implies that the 2D cross-section of the source-receiver plane for the 3D configuration is modeled by a 2D calculation. The 3D results are obtained by using the 2.5D approach based on 2D calculations as in Ref. 9. For the source position in the middle of the street, and horizontal receiver coordinates $(x, \tan(\theta))$, the projected 2D receiver distance is $x_\perp = |\vec{x}_\perp| = x/\cos(\theta)$ and the projected source canyon width $W_\perp = W/\cos(\theta)$. Figure 9 shows the broadband $A'_{s,2D}$ and A'_s results for $x=10W$ as a function of the angle θ. In 3D, $A'_s = A_s - 20\log_{10}\left(\left|\vec{x}_\perp - \vec{x}_{ES,ref,\perp}\right|/\left|\vec{x}_\perp - \vec{x}_{ES,\perp}\right|\right)$, and here $\vec{x}_{ES,ref,\perp} = (0,0)$ and $\vec{x}_{ES,\perp} = (-W,0)$.

Two 3D results are shown in Figure 9, with different calculations of the reference configuration s,ref. The results denoted by *3D* are computed with a reference calculation using the Hadden and Pierce model accounting for the oblique angle between the diffraction edge and the source-receiver direction. The results denoted by *3D projected ref* are computed with a reference calculation using the Hadden and Pierce model where the diffraction edge is perpendicular to the source-receiver direction. The use of the latter reference configuration is according to the approach in standard engineering methods.[6] Results show that the angular dependence for the *2D projected* case and the *3D* case is weak, and methods deviate significantly only for the largest angles, i.e. above 70°. The *3D projected ref* results exhibit a higher dependence and do deviate more from the *2D projected* results. In fact, the differences between the *3D* and *3D projected ref* results reflect the error from computing configuration s,ref without accounting for the oblique angle between the diffraction edge and the source-receiver direction, at least up to 70°. When computing $A'_{s,2D}$ and assuming that $A'_{s,2D} \approx A'_s$, the error introduced by the edge diffraction model for $\theta > 0$, which is present in current engineering methods, thus remains.

4   CONCLUSIONS

A recently proposed improved engineering method for urban areas shielded from direct exposure to traffic noise include terms that account for multiple reflections of the built environment in the source and receiver area. These separate terms, A_s and A_r, rely on 2D source-receiver propagation calculations using a wave-based acoustic propagation method. In this work, the validity of this approach has been investigated. For this purpose, calculations with a wave-based calculation model have been carried out.

It can be concluded that, when averaging over receiver position in a shielded canyon environment, the terms A_s and A_r may be used independent from each other for canyon-to-canyon distances exceeding $2W$, where W is the canyon width. For shorter distances, the effects of source and receiver environment should be computed as a single term A_{can}. For source-receiver distances exceeding $4W$, results support the use of distance independent values of A'_s and A'_r and additional analytical expressions to account for distance dependence.

For source-receiver distances exceeding $2W$, and propagation angles normal to street façades, the terms A'_s and A'_r are very similar in 2D and 3D, supporting the use of 2D calculations. For source-receiver propagation angles deviating from the normal to the street canyon axis and below 70°, A'_s and A'_r are rather independent on the angle, and 2D results may be used to define A'_s and A'_r too. For propagation angles exceeding 70°, 2D results start to deviate from the 3D results. However, for such propagation angles, it is unlikely that the results are not affected by cross streets or the finiteness of the street canyon. Calculations also identify that for wave propagation with oblique incidence to street façades, the edge diffraction calculation assuming that street façades are normal to the source-receiver direction, as common in engineering methods, leads to too low levels. By computing A'_s and A'_r based on 2D calculations, this error is not corrected for.

Further work will focus on the assessing the assumption $A'_{s,2D} \approx A'_s$ and $A'_{r,2D} \approx A'_r$ for configurations such as courtyards and street canyons interrupted by cross streets.

5   ACKNOWLEDGEMENTS

6   REFERENCES

1. Directive 2002/49/EC of the European Parliament and of the Council relating to the assessment and management of environmental noise, (2002).
2. W. Wei, T. Van Renteghem, D. Botteldooren, M. Hornikx, J. Forssén, E. Salomons and M. Ögren, "An efficient model for background noise mapping", in Proc. of EURONOISE 2012, 10-13 June, Prague, Czech Republic, (2012).
3. T. Kihlman, M. Ögren and W. Kropp, "Prediction of urban traffic noise in shielded courtyards", in Proc. of The Int. Cong. and Exp. on Noise Control Eng., Dearborn, MI, USA, (2002).
4. M. Ögren and W. Kropp, "Road traffic noise propagation between two dimensional city canyons using an equivalent source approach", *Acta Acust. United Ac.* **90**(2), (2004).
5. M. Hornikx, R. Waxler and J. Forssén, "The extended Fourier pseudospectral time-domain method for atmospheric sound propagation", *J. Acoust. Soc. Am.*, **128**(4), (2010).

6. E. Salomons, D. van Maercke, J. Defrance and F. de Roo, "The Harmonoise Sound Propagation Model", *Acta Acust. United Ac.* **97**(1), (2011)

7. J. W. Hadden and A. D. Pierce, "Sound diffraction around screens and wedges for arbitrary point source locations", *J. Acoust. Soc. Am.*, **69**(5)**,** (1981). Erratum (1982), J. Acoust. Soc. Am. **71**(5).

8. T. Van Renterghem, E. Salomons and D. Botteldooren, "Efficient FDTD-PE model for sound propagation in situations with complex obstacles and wind profiles," *Acta Acust. United Ac.* **91**(4), (2005).

9. M. Hornikx and J. Forssén, "The 2.5-dimensional equivalent sources method for directly exposed and shielded urban canyons", *J. Acoust. Soc. Am.*, **122**(5), (2007).
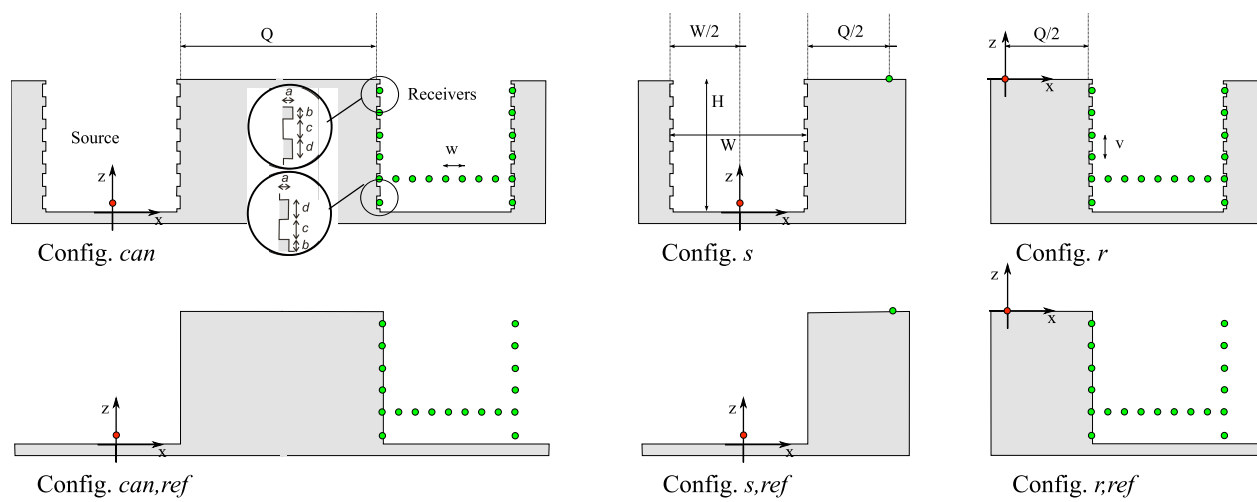
Fig.1 - *Configurations studied, a=0.16 m, b=0.64 m, c=1.92 m, d=1.28 m, v=c+d=3.2 m, w=1.6 m, z_s=0.5 m, W=19.2 m, H=19.2 m, Q is variable.*
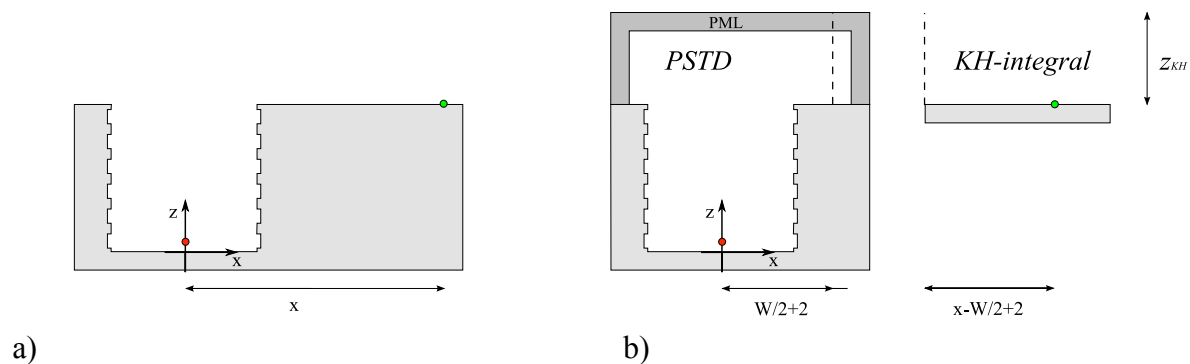
Fig. 2 - *Two-step numerical approach to solve configuration of a), b) Application of PSTD method to solve source region part, and evaluation of the KH-integral equation to solve the region over roof level height.*
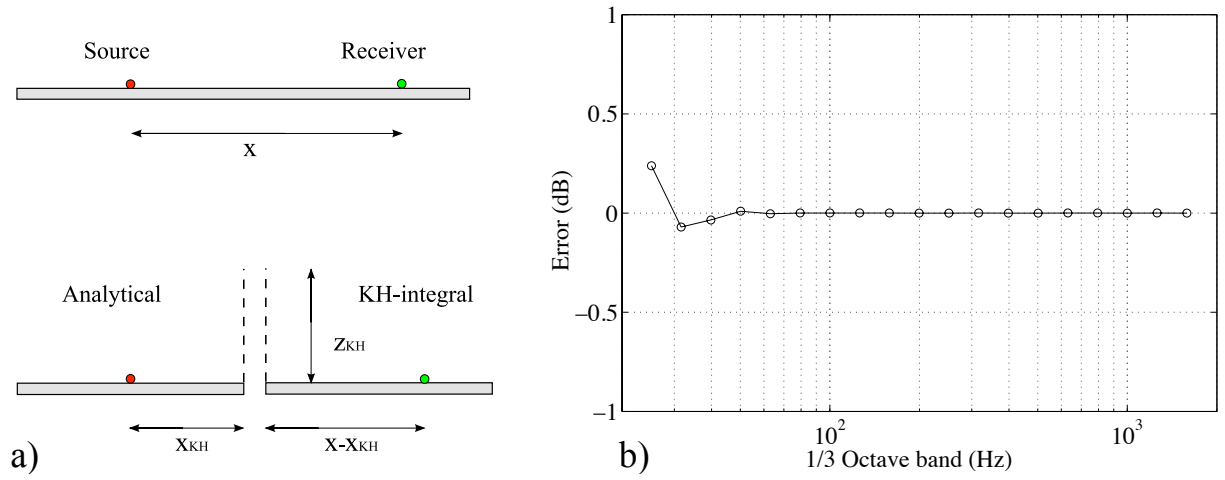
Fig. 3 - a) upper) Configuration studied, lower) two-stage computational approach with analytical results at $x=x_{KH}$ and KH-integral approach from $x=x_{KH}$ to receiver. b) Error of the KH-integral approach for $z_{KH}=29.6$ m, $x_{KH}=11.6$ m and $x=200$ m.
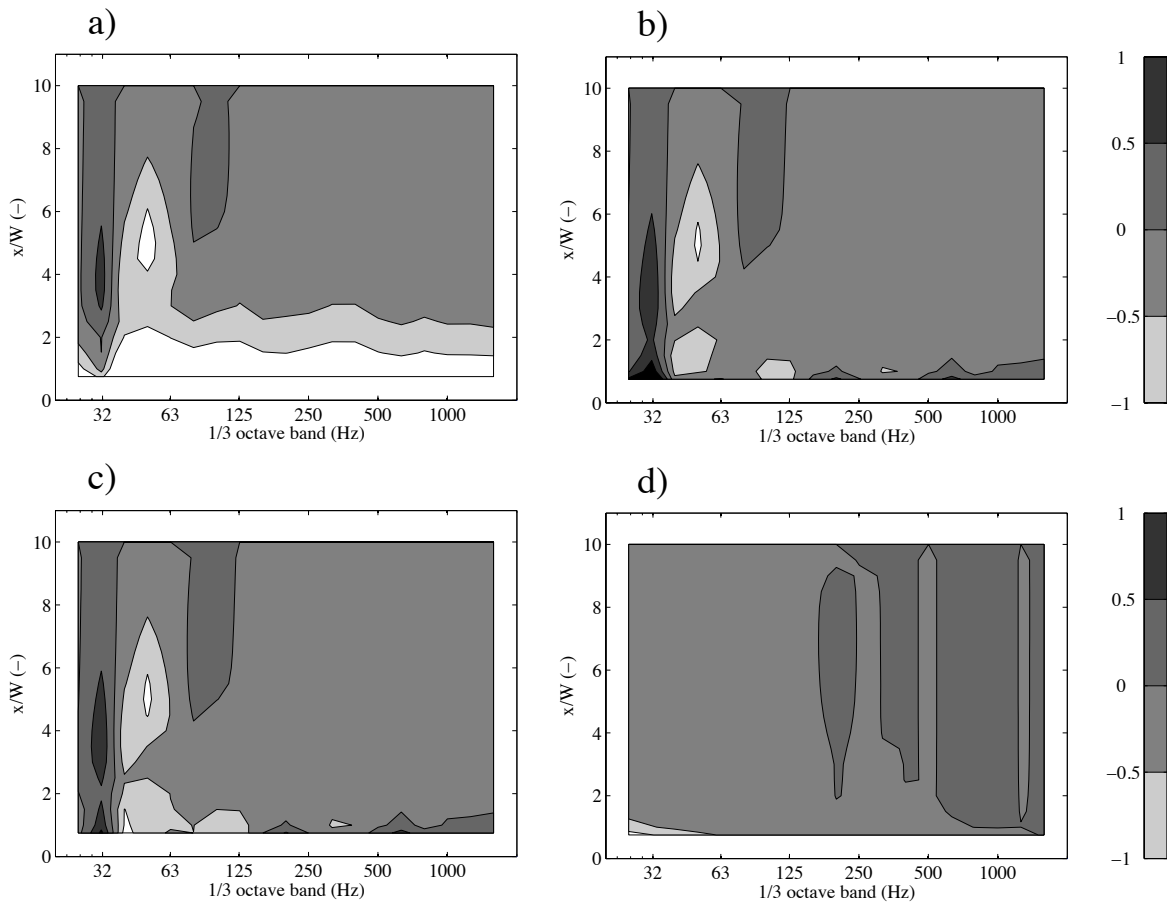

Fig. 4 – Attenuation terms in dB computed for configuration s and s,ref of Figure 1), a) $\Delta A_{s,2D}$, b) $\Delta A'_{s,2D}$, c) $\Delta B_{s,2D}$, d) $\Delta B_{s,2D,ref}$
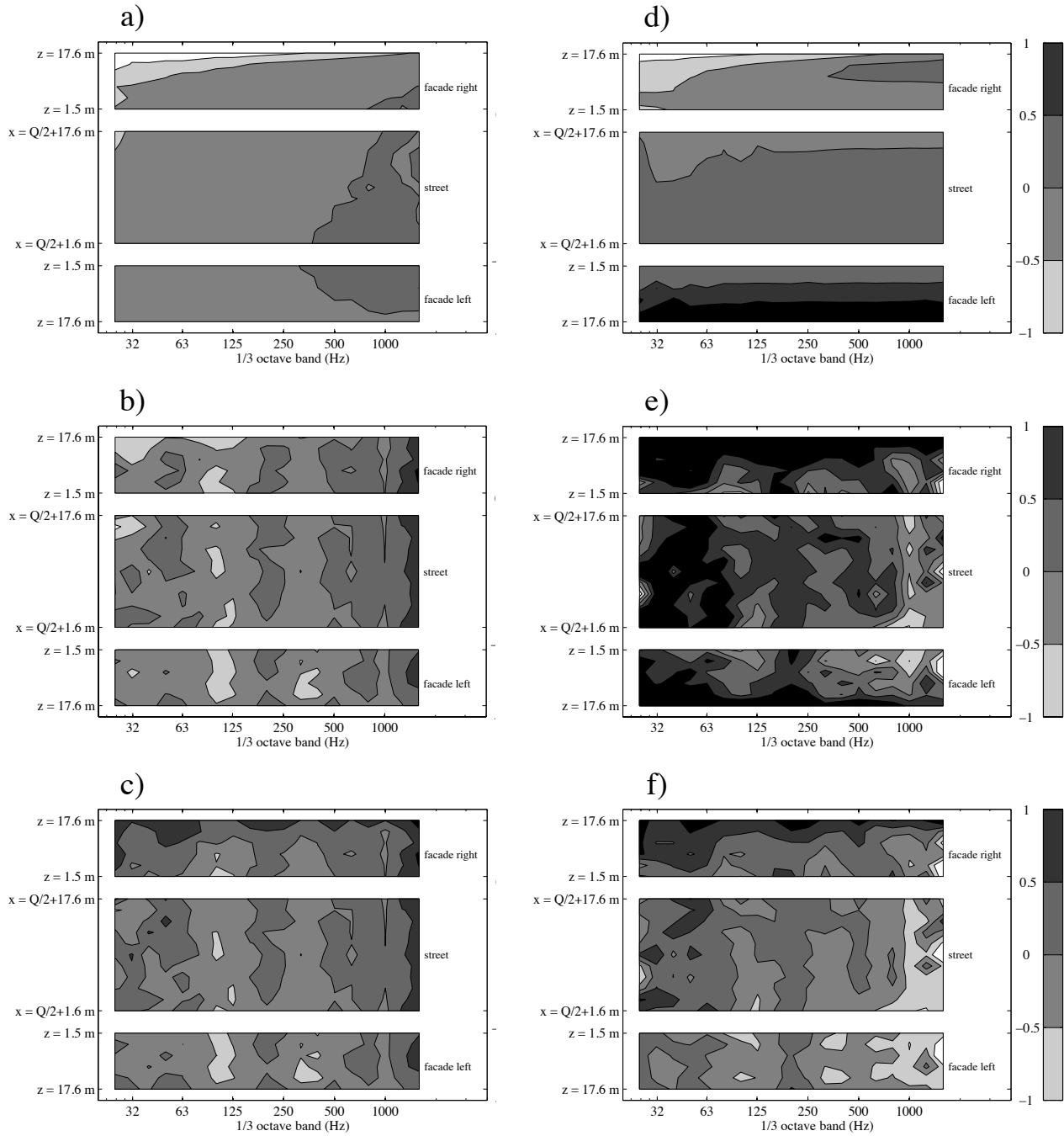
Fig. 5 - *Attenuation terms in dB computed for configuration r and r,ref as a function of receiver positions from Figure 1, a) $\Delta B_{r,ref,2D}(2W)$, b) $\Delta B_{r,2D}(2W)$, c) $\Delta A'_{r,2D}(2W)$, d) $\Delta B_{r,ref}(2W)$, e) $\Delta B_r(2W)$, f) $\Delta A'_r(4W)$.*
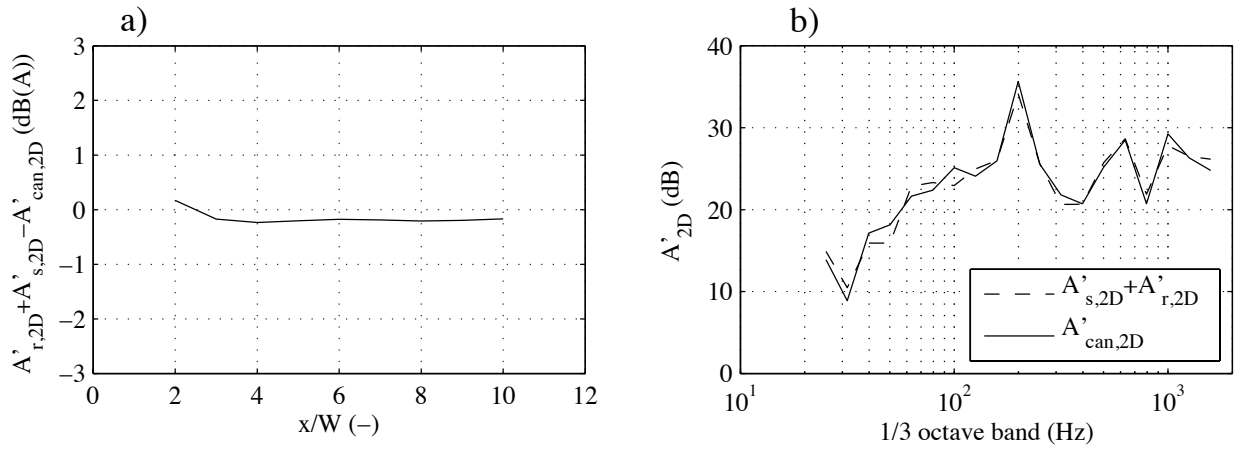
Fig 6 - a) Broadband error of splitting the attenuation term $A'_{can,2D}$ into $A'_{s,2D} + A'_{r,2D}$. Results have been averaged over all receiver positions, b) A'_{2D} results averaged over all receiver positions.
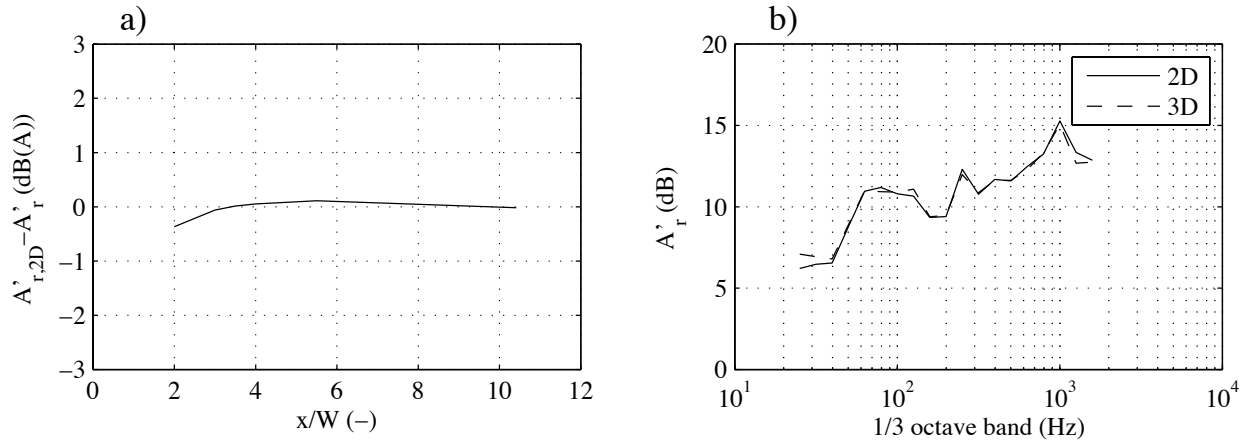

Fig 7 - a) Broadband difference between the attenuation terms $A'_{r,2D}$ and A'_r. Results have been averaged over all receiver positions, b) $A'_r(10W)$ results averaged over all receiver positions.
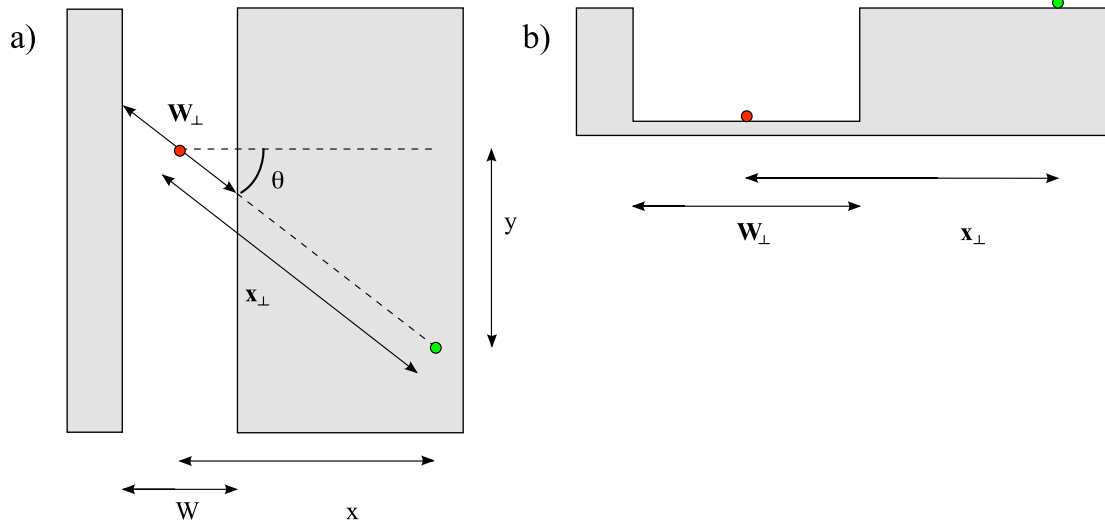
Fig. 8 - a) Top view of configuration s of Figure 1 for θ ≥0°. b) Projected 2D approach of a).
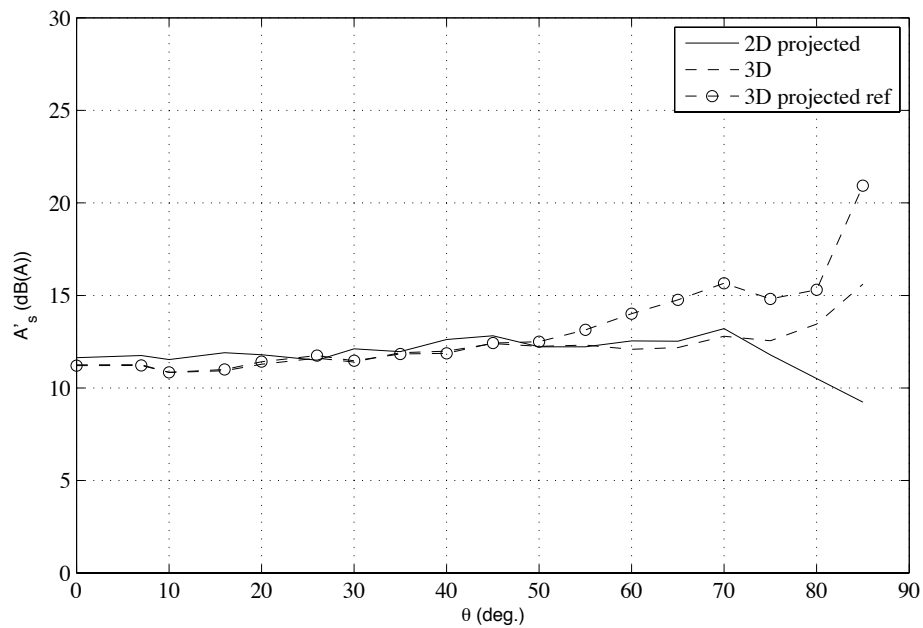

Fig. 9 - Broadband A'$_s$(x=10W) results for configuration s as depicted in Figure 8. 3D projected ref corresponds to a calculation for configuration s,ref with the diffraction edge normal to the source-receiver direction for all angles θ.